ID14 'Quadriga', a Beamline for Protein Crystallography at the ESRF

S. Wakatsuki,[a]* H. Belrhali,[a] E. P. Mitchell,[a] W. P. Burmeister,[a] S. M. McSweeney,[b] R. Kahn,[c] D. Bourgeois,[c] M. Yao,[d,e] T. Tomizaki[a] and P. Theveneau[a]

[a]*ESRF, BP 200, F-38043 Grenoble CEDEX, France,* [b]*EMBL Outstation, BP 156, F-38042 Grenoble CEDEX, France,* [c]*IBS, 41 Avenue des Martyrs, F-38027 Grenoble CEDEX, France,* [d]*MacScience, Yokohama, Japan, and* [e]*Osaka University, Osaka, Japan.*
E-mail: wakatsuki@esrf.fr

The ESRF undulator beamline ID14 'Quadriga' is dedicated to monochromatic macromolecular crystallography. Using two undulators with 23 mm and 42 mm periods and a minimum gap of 16 mm installed on a high-β section, it will provide high-brilliance X-ray beams at around 13.5 keV, as well as a wide tuneability between 6.8 and 40 keV. Based on the Troika concept, this beamline has four simultaneously operating experimental stations: three side stations, EH1, EH2 and EH3, using thin diamond crystals, and an end station, EH4, with a fast-scan double-crystal monochromator. Station EH3 has a κ-diffractometer, and an off-line Weissenberg camera with a large 80×80 cm active area combined with a 2048×2048 CCD detector. During data collection the image plates are placed and removed by a robot located inside the hutch using a cassette system. After data collection the image plates are scanned with an off-line drum scanner. Station EH4 is designed for MAD applications, including Xe K-edge anomalous experiments, and is equipped with a 2048×2048 CCD detector on a pseudo 2θ arm. A common graphical user interface and a database will be available to cover all aspects of data collection, including strategy optimization. First results on the performance of the optics elements and initial crystallographic results are presented.

Keywords: protein crystallography; diamond optics; MAD; Weissenberg cameras; imaging plates.

1. Introduction

Using the high brilliance of X-ray beams from undulators on third-generation synchrotron sources, it is now possible to collect X-ray diffraction data either from microcrystals of proteins with smallest dimensions of 5–10 µm or from crystals of extremely large proteins or viruses (unit cells up to 1500 Å). This is largely due to the high brilliance and low emittance of undulator beams combined with state-of-the-art focusing optics. Since the opening of the ESRF to the macromolecular crystallography community, these features have been fully exploited. The macromolecular crystallography beamline, ID14 'Quadriga', is one of the six ESRF beamlines that study biological macromolecules by crystallography. The current experimental stations, with the exception of BM14, are only partially dedicated to macromolecular crystallography (ID2, ID9, ID13, BM2) and all are heavily oversubscribed. Additional stations are needed and to serve this demand, ID14A/B has been designed to have four end stations operating simultaneously using just one straight section of the storage ring.

Using two undulators on a high-β section, the beamline provides high-brilliance X-ray beams at around 13.5 keV, as well as wide tuneability between 7 and 40 keV on the last station. Based on the Troika concept (Grübel *et al.*, 1994), the beamline has four stations: three side stations using transparent diamond crystals and an end station with a double-crystal monochromator (Figs. 1 and 2). These stations will be operated independently to allow four different user groups to collect protein crystallography data simultaneously. The end station can be used for MAD applications. The beamline is being constructed in two stages, starting with the optics hutches and the two downstream stations, operational in late 1997, followed by the addition of the remaining two side stations in 1998. This paper describes the current status of the beamline as of late-summer 1997.

2. Undulator source and optics

2.1. Undulator source

The beamline has two undulators, each with a minimum gap of 16 mm and a length of 1.65 m. The first undulator,

with a periodicity of 42 mm, is tuneable over a wide wavelength range and will be used to provide X-rays for experiments outside the standard energy range of 11.5 to 13.5 keV. The second undulator, with a periodicity of 23 mm, is a single-line undulator with very little tuneability but optimized for giving the highest brilliance at around 13.5 keV, which is above most of the relevant absorption edges in protein crystallography (Se, Br, Pt, Au, Hg, Pb, to name but a few). As this undulator induces only a small additional heat load on optical elements, it is operated in tandem with the 42 mm undulator.

2.2. Diamond optics

The diamond optics are essential for delivering high-brilliance X-ray beams to the three experimental side stations. The absorption of X-ray photons which do not fulfil the Bragg condition is low. The excellent thermal properties of diamond also solve the problem of the high
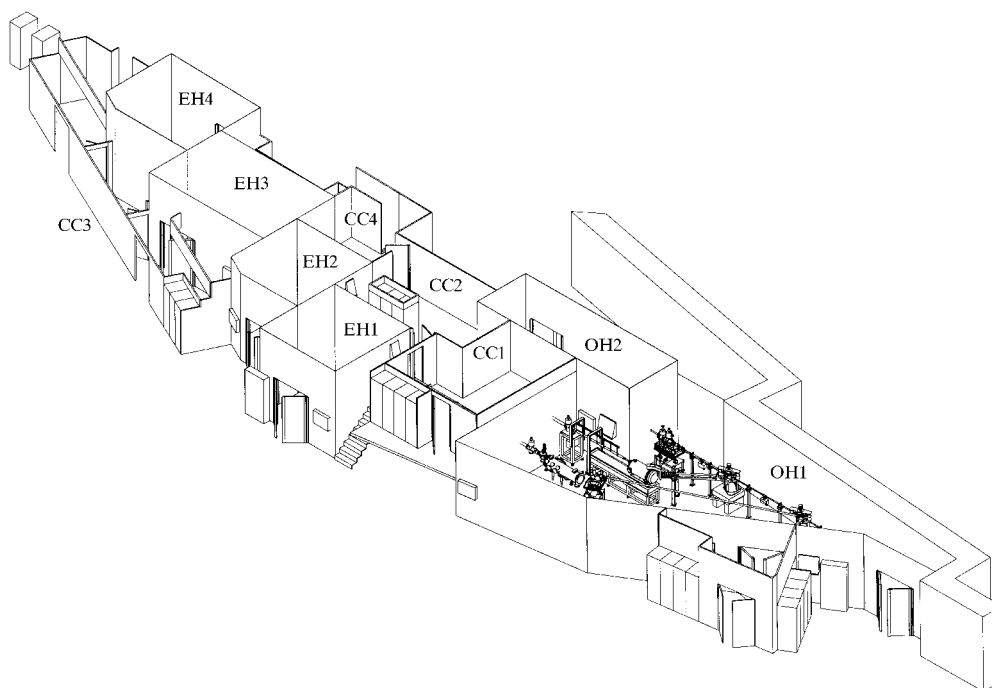
Figure 1
Layout of the four stations, three with diamond monochromators, second monochromators (and multilayer), and one end station. OH1: first optics hutch for pre-pump, primary, secondary slits, three diamond monochromators, and chambers for second monochromator crystals and mirrors. OH2: second optics hutch for the end station. EH1–EH4: experimental hutches. CC1–CC4: control hutches for users.
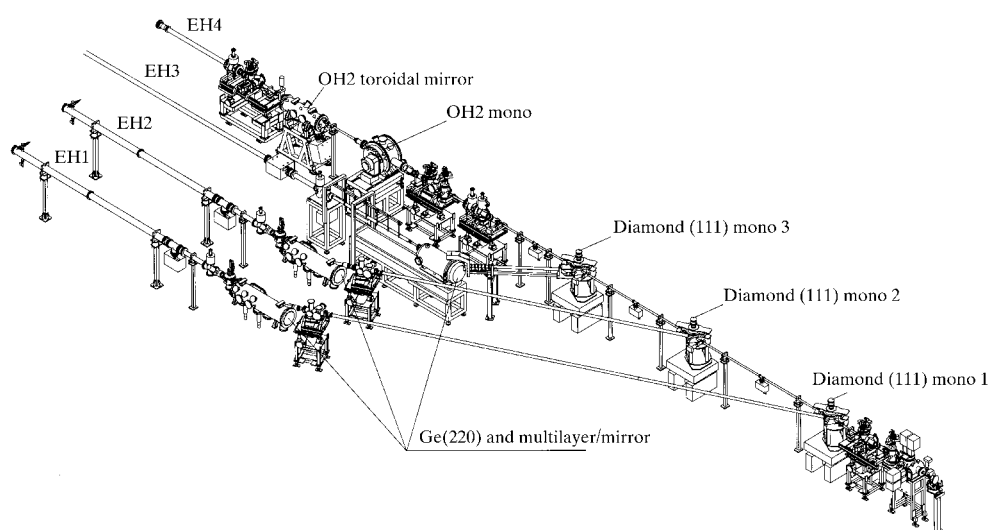
Figure 2
Layout of the optics. Walls of the optics hutches are not shown.

power density of the undulator beam. In order to have the highest possible flux we chose the diamond (111) reflection. Reflectivity measurements on crystals in symmetric Bragg mode and in asymmetric Laue geometry showed that the asymmetric Laue crystals cut along the (100) axis crystals behave almost like perfect crystals and have an integrated reflectivity comparable with that of the symmetric Bragg (111) crystals (Burmeister *et al.*, 1997), although in theory Bragg crystals should have a twofold-higher reflectivity. A number of yellow type-Ib (100) diamond crystals with a size of up to 7 × 7 mm and a thickness of 0.1 mm are available. Such a crystal has been used in the commissioning experiment described below.

Our ultimate goal is to use (111) diamonds in Bragg mode. This means that the crystals have to be thinner than 100 µm in order to avoid significant attenuation of the main beam for the downstream stations, as the path of the white beam is around four times as long as the path in the asymmetric Laue crystals. Large-size (111)-oriented diamond slabs with the required perfection are still rare. It is difficult to cleave or polish those which do exist to a thickness of less than 100 µm. The possibility of laser ablation of (111) diamond crystals is being investigated to thin down part of a large diamond crystal (6 × 10 mm) to a thickness of ~50 µm. Other collaborations aim to improve the surface quality of the crystals. The rocking curve of the (111) reflection from the (100) oriented monochromator crystal has been measured. At an X-ray energy of 13.5 keV the FWHM of the reflection was 3.2 mdeg, analysed with a Ge(220) crystal, compared with the theoretical value of 2.2 mdeg (Fig. 3).

The complete diamond monochromator, vessel and mechanics for EH3 have been designed and constructed in-house (Mattenet *et al.*, 1998). Two further monochromators for EH1 and EH2 are being currently manufactured.

In order to minimize the number of energy gaps due to the simultaneous excitation of reflections at different energies, a computer program has been developed to investigate the optimum orientations of the diamond monochromator crystals. The predicted energy gaps have been verified experimentally and it was found that the [010] axis of [111] Bragg crystals should be inclined by 30° from the vertical to minimize the number of energy gaps in the energy range 7–14 keV.

2.3. Beam focusing for EH3

The beam reflected from the diamond crystal is reflected again by a second crystal, a sagitally bent Ge(220) crystal of radius 6–10 m for vertical focusing. The crystal also restores a beam direction almost parallel to the main beam but 2 m apart. The third optical element, a bent multilayer, focuses the beam in the horizontal direction and rejects higher harmonics (Als-Nielsen *et al.*, 1994).

The multilayer consists of a silicon substrate on a bimorph piezoelectric ceramic material. It is coated with 100 layers of ruthenium and boron carbide with a *d*-

spacing of 68 Å. Recent commissioning tests have shown that the multilayer has a reflectivity of approximately 65% at 13.5 keV. The multilayer is bent by applying a high voltage to the bimorph material. This leads to an easy method of focusing; the position of the exit beam remains unaffected using a specially designed holder for the bimorph.

The optical system is designed to be tuneable between 8.2 and 13.8 keV. To achieve this, the second monochromator crystal and multilayer are translated along the beam by up to 2 m in order to follow the beam reflected from the diamond. A motorized bender for the sagittal focusing germanium crystal and voltage-controlled bimorph bender for the multilayer allow the beam focus to be optimized at all energies.

The stability of the X-ray beam, both in intensity and position, is crucial to the success of user experiments. Precise temperature control of the experimental hutch and heavy granite supports for the optical elements serve to maintain a stable beam intensity. So far, the monochromatic beam has been insensitive to the variations of heat load during a fill cycle. A similar experiment measuring the X-ray intensity at the sample position (behind 0.3 × 0.3 mm slits) in the experimental hutch gave encouraging results. In this case the beam was monitored after the diamond/Ge monochromator (Ge crystal unbent) and the focusing multilayer element.

2.4. Second optics hutch, OH2

Since the diamond monochromators are essentially transparent, the optics used in this hutch must withstand the power input from the undulators. For this reason the first optical element in OH2 is a cryocooled double-crystal monochromator with symmetrically and asymmetrically cut Si(111) and Si(311) crystals. The monochromator is
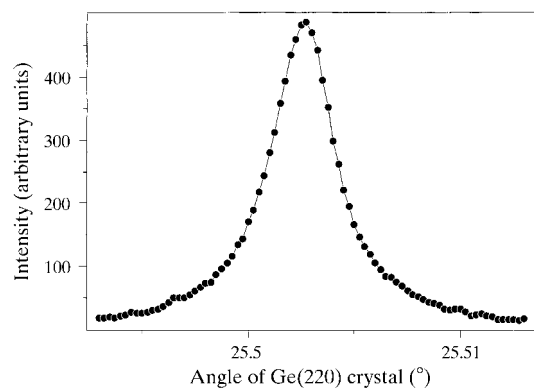
Figure 3
Rocking-curve measurement of type Ib (100) diamond crystal using Ge(220) as an analyser crystal. The two undulators were operated: U23 16.3 mm, and U42 17.11 mm. The beam current was 134 mA with 3 × 3 mm slits after two absorbers, 2.5 mm of carbon and 1 mm of aluminium. The theoretical rocking-curve widths of diamond (111) and Ge(220) reflections are 0.9 mdeg and 1.9 mdeg, respectively, at 13.5 keV, which gives rise to a convoluted rocking-curve width of 2.2 mdeg (Sanchez del Rio & Dejus, 1998).

capable of rapidly tuning the X-ray energy with a fast $(0.5° \text{s}^{-1})$ rotation of the monochromator crystals. This is essential when the white beam has to be analysed for glitches produced by the upstream diamond monochromators. The X-ray beam is focused using an uncooled toroidal mirror situated at 47 m from the source. The toroid shape is chosen to provide the optimal focus at the sample position in EH4, at a distance of 67 m. The mirror is 80 cm long and coated with rhodium in order to avoid absorption edges in the energy range between 10 and 15 keV. Ray tracing indicates that a focal spot of size $0.5 × 0.4$ mm FWHM will be achievable.

3. Experimental stations

Using the diamond optics, the four experimental stations will be operated simultaneously. The first three stations will use slightly different wavelengths so that they do not interfere with one another. The wavelength used for EH3 will stay fixed for a given period of time (1 day for example) whereas those for EH1 and EH2 will be fixed. Since the rocking-curve widths of the diamond optics are very narrow, a few eV, the wavelengths of the first three stations can be almost identical, as close as 0.001 Å. Our aim is to provide four user groups with similar experimental environments, such as crystal viewing apparatus, cryo set-ups, detectors, data acquisition and data analysis. While the first two stations are designed for fixed-wavelength experiments, EH3 is specialized for large structures and EH4 for MAD experiments.

3.1. *Experimental stations EH1 and EH2*

These stations will be the final branch lines constructed. They are currently being designed and construction in the optics hutch will start in early 1998. The optical design of the stations will take elements from EH3, and use experience gained from the EH3 commissioning. However,
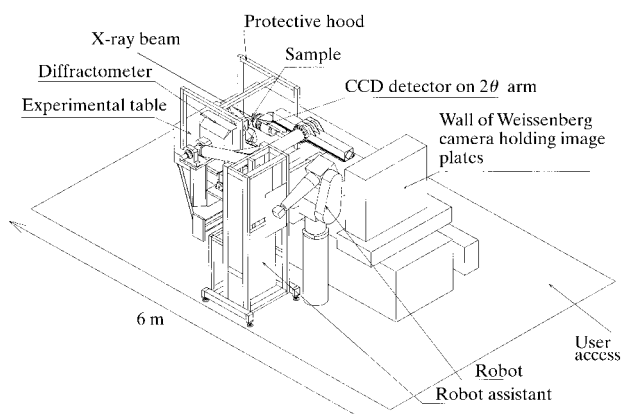
both EH1 and EH2 will operate at the peak brilliance of the 23 mm undulator, which is close to 0.92 Å. Stability in the optical design is still a major concern, with 9 m and 13 m between the diamonds and second crystals for EH2 and EH1, respectively. With this in mind, the two designs are being kept as simple as possible.

The EH2 branch will use the (220) reflection from a flat germanium crystal as the second monochromator stage, followed by a toroidal mirror. The mirror will have a fixed shape. Since the energy is non-tuneable, a mirror of fixed shape offers the simplest approach as well as being more economical than a mirror plus bender. Station EH1 will use the same layout as EH3 with a sagitally focusing germanium (or silicon) crystal and a multilayer on a bimorph bender as optical elements. These will be at fixed positions and not mobile like those of EH3.

The experimental hutches, EH1 and EH2, will be equipped initially with CCD detectors and single-axis φ-spindle goniometers.

3.2. *Experimental station EH3 with Weissenberg camera*

The experimental station EH3 is equipped with a four-circle κ-diffractometer with a horizontal ω axis, a tapered fibre-optics coupled CCD detector on a 2θ arm, the Weissenberg camera with an optional helium chamber, a cryostream and a removable enclosure to carry out P2-level biohazardous experiments (Fig. 4). The wall of the Weissenberg camera can hold one or two $40 × 80$ cm image plates, thus forming a maximum active area of $80 × 80$ cm, or $8000 × 8000$ pixels. The distance between the crystal and the image plates can be varied from 360 to 2000 mm. Without human intervention during the course of one data set, a robot inside the hutch transfers the image plates from a cassette, containing up to 16 image plates, to the camera with the help of another device called a robot assistant. Image plates and cassettes carry bar codes and their numbers are used in an image-plate database. The database is linked to the camera, the scanner and the robot assistant, allowing fully automated image-plate management during an experiment. With this set-up, many image plates are exposed as fast as possible, without the delay of interlocking procedures; they are read off-line afterwards.

The flat image-plate camera can be translated along any direction perpendicular to the X-ray beam. With knowledge of the lattice, the cell dimensions and the orientation of a crystal in the beam, optimal coupling constants between the Weissenberg translation and the spindle as well as the maximum oscillation range are calculated to avoid overlap of diffraction spots. This unique synchronization of the two-dimensional Weissenberg motion and the spindle allows a more efficient use of the detector active area and therefore a smaller number of oscillation frames to collect a complete data set.

The second area detector is a tapered fibre-optics coupled CCD system which will be used for quick assess-

Figure 4
Schematic diagram of the experimental station ID14/EH3. The Weissenberg camera and the robot installed in the experimental hutch are shown together with an alignment table, the diffractometer, the CCD detector and the robot assistant.

ment of crystal quality, the decay of the diffraction patterns during off-line imaging-plate data collection, as well as for the alignment of the crystal and the determination of the parameters for the Weissenberg exposure. The CCD detector is installed on a 2θ arm so that it can be moved in and out of the data-collection position remotely. In operation without the Weissenberg camera it can be used for data collection on protein crystals (see below).

The scanner is designed to read a number of image plates automatically from a cassette holding up to 16 40×80 cm image plates (Cipriani *et al.*, 1997). Each image plate is picked up from the cassette with a suction cup, rolled onto a cylindrical drum and held by vacuum. Each image plate is identified by a bar code, and its relevant information, such as the status of the image plate, is checked with the database. After scanning, the image plate is put back into the cassette and the image-plate database is updated. This process is repeated until all the image plates are scanned.

3.3. Experimental station EH4 for MAD

The equipment in this experimental hutch will be able to use fully the high intensity of the undulator beam. A κ-four-circle diffractometer, identical to that in EH3, is combined with a pseudo 2θ arm for the CCD detector. The pseudo 2θ arm consists of a 1 m-long translation stage on which vertical translation and tilt stages are mounted to make a pseudo 2θ motion. The CCD systems (MAR, USA) are based on single 2048×2048 pixel chips coupled with tapered fibre optics. The active area has a diameter of 133 mm. The readout time is about 20 s (6 s to read the image into the memory using 16-bit ADCs, 2 s to transfer to a hard disk, and an additional 7 s for correction of spatial distortion and non-uniformity of the detector response). The detectors are controlled by Pentium PCs running Linux. The diffractometer will be linked to 'intelligent' software to allow flexible and rapid data collection. For experiments using extremely short wavelengths, for example the Xe K-edge, the focusing mirror is dropped out of the beam and an unfocused beam will be used. The height of the experiment table can be changed quickly for this purpose.

3.4. Sample preparation facility

For efficient use of synchrotron beamtime, it is essential to have a sample preparation laboratory near the experimental hutches. A sample preparation area is being built near the beamline, which will be used for preparing heavy-atom derivatives, pre-freezing of samples for the four stations, and as a crystal-mounting area for EH1. In addition, EH2 has a small sample preparation area in front of the experimental hutch, and EH3 will use one of its control cabins for mounting crystals. EH4 will share a sample preparation laboratory with BM14, the MAD beamline adjacent to EH4/ID14. There are also more comprehensive biochemical facilities available for users at the EMBL Grenoble Outstation.

4. Data acquisition and analysis

The major part of the experimental stations are controlled by Hewlett-Packard (HP) UNIX workstations with VME electronics using the operating system OS9 and SPEC for instrumentation control. Data-acquisition computers vary according to the detectors: Pentium PCs running Linux for the CCD detectors and an HP workstation for the image-plate scanner. For data analysis, each station is equipped with a pair of Silicon Graphics O2 and O200 computers for on-line data processing. The beamline computers are connected to the ESRF central computing facility, NICE, *via* an ATM network. The bulk of the data can be stored on NICE systems as well as on the beamline computers. It is envisaged that the beamline computers will be used for on-line data processing. This will range from assessing data quality and completeness to processing fully data and calculating electron density maps. The estimated rate of raw data production will be 1–2 GB day^{-1} station^{-1} up to 150 GB day^{-1} station^{-1}, depending on the experiments carried out.

We are developing a comprehensive software package, *ProD*C, for beamline control, data acquisition and data analysis, in order to fulfil the following requirements of the beamline. (i) On-line data analysis runs automatically as the images are collected and keeps track of the data acquisition so that users know the quality of the data, completeness *etc.* (ii) A graphical user interface will be able to interact with different processes (beamline control, data acquisition and data analysis) running on different computers at different times. (iii) Optimum data-collection strategies based on cell dimensions, crystal orientation and space group can be suggested. These strategy solutions include orienting the crystal for optimizing anomalous signals, knowing all the geometrical constraints of the κ-diffractometer including beamstop, cryosystem and collimator. If one or more data sets have already been collected from other crystals, the strategy program will suggest the best strategy to fill the missing region of the previous data sets. The strategy can be updated while the data set is collected. (iv) The graphical user interface is interfaced to widely used processing programs such as *DENZO*, *SCALEPACK*, *MOSFLM* and other *CCP4* programs with common graphical representation of results. (v) A database will be implemented in order to deal with the high volume of data that will, in principle, be produced by the beamline. *ProD*C has been installed on ID2 (PX), and used successfully for a year and a half.

The data-collection strategy program (Yao *et al.*, in preparation) is intended for various diffractometer geometries, including single-spindle, κ- and Eulerian four-circle diffractometers, with the ω axis either in the horizontal or vertical direction. The program can import cell parameters and an orientation matrix from an output file

of either *MOSFLM* or *DENZO* and calculates the best data-collection strategy for simultaneous measurements of Friedel pairs, high completeness or uniform redundancy. It can also suggest a strategy to fill in missing data from previously collected data sets. It is now being implemented into *ProD*C.

5. First structural results and discussions

During the limited time for collecting diffraction data before the summer shutdown, diffraction data were recorded from several crystals, including those of myrosinase, luciferase and tropinon reductase II. For this purpose we used a single-spindle axis with a primitive synchronization protocol with the X-ray shutter. Diffraction data were collected on 40×80 cm image plates (one imaging plate for each oscillation) without Weissenberg motions. At this stage, the robot and the robot assistant were not ready, and therefore the imaging plates were changed manually. The protein crystals were tested at room temperature and diffracted well. An example of a diffraction pattern is shown in Fig. 5. Data were processed with the *HKL* package (Otwinowski, 1993) and *CCP*4
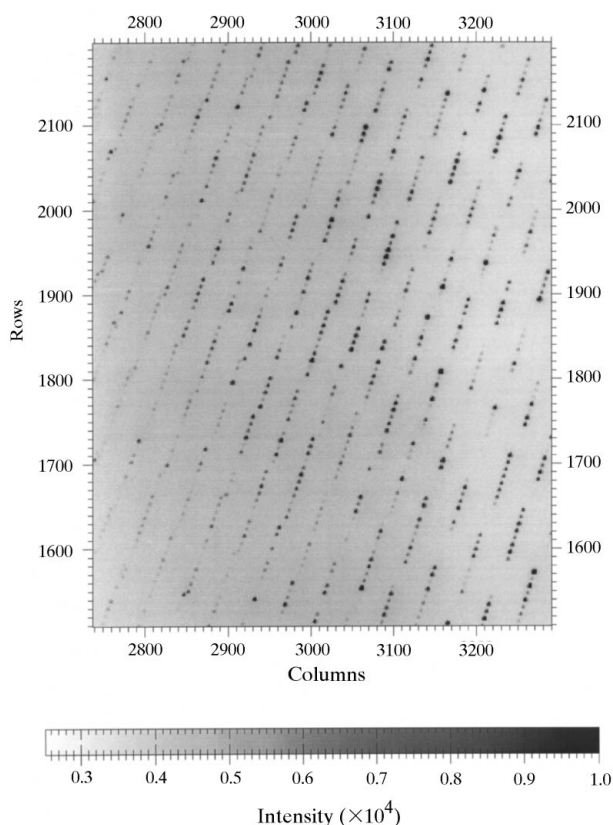
Figure 5
A section of a diffraction image of a tropinone reductase II crystal (space group $P6_122$, $a = 89.7$ Å, $b = 89.7$ Å, $c = 340.2$ Å) taken on EH3/ID14. The exposure time was 120 s for a 3° oscillation. The image plate was scanned with 100 µm raster which gives 4000×8000 pixels (64 Mbytes). The crystal-to-detector distance was 360 mm and the wavelength was 0.918 Å.

suite (Collaborative Computational Project, Number 4, 1994).

The first crystal tried on EH3 was an orthorhombic myrosinase (Burmeister *et al.*, 1997) crystal from which only 14° of data were collected at room temperature. This is the reason for the low completeness of 21.6%. Nevertheless, the quality of the diffraction data was quite acceptable ($R_{\mathrm{merge}} = 3.7\%$ over all data to 1.6 Å). The second crystal was of tropinon reductase II with a *c* axis of 340 Å. The spots along the *c* axis were well separated on the image plate. The diffraction spots were clearly observed beyond 1.8 Å, whereas, on a rotating anode, spots barely reached 2.5 Å and could not be processed due to the long cell dimension (Fig. 5). This data set was further analysed and the structure was solved at 1.9 Å resolution with molecular replacement (Yamashita *et al.*, 1998). Part of the $2F_o - F_c$ electron density map, around tyorosine Y155, is shown in Fig. 6.

The large number of pixels, 8000×8000, of the Weissenberg camera allows us to collect data from extremely large macromolecules or from crystals which diffract to very high resolution. For example, at a wavelength of 0.92 Å and a crystal-to-detector distance of 1000 mm, the edge of the camera corresponds to 2.4 Å resolution. In this set-up, diffraction spots from a blue tongue virus crystal, with the longest cell parameter of 1592 Å, would be separated by 0.57 mm (5.7 pixels). These spots can be resolved provided that the mosaicity is small. At the other extreme, using a crystal-to-detector distance of 360 mm and an X-ray wavelength of 0.92 Å, the Weissenberg camera can collect data up to 1.1 Å resolution.

Once operational, the image-plate scanner, together with the rest of the data-acquisition system, will provide a unique facility for collecting macromolecular crystallographic data from extremely large molecules. Using these instruments, it will be possible to screen good crystals from the crystallization batches using the CCD detector and, once finding a good crystal, to collect a
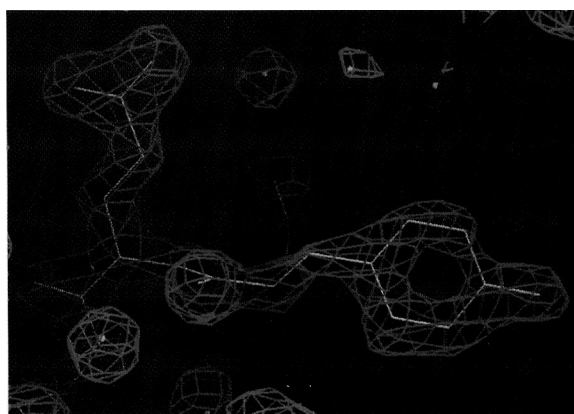
Figure 6
Part of the $2F_o - F_c$ electron density map of tropinone reductase II showing a tyrosine residue, Y155. The contours were drawn at a 2σ level from the map calculated using data between 10 and 1.9 Å.

complete data set with image plates before the crystal is damaged by the X-ray beam with optimized experimental parameters for the Weissenberg camera. This is especially relevant for virus crystals, which often cannot be frozen and thus are subject to extensive radiation damage.

6. Conclusions

The construction and commissioning of the beamline have proceeded significantly over the past two years and now have reached a stage where the two experimental stations, EH3 and EH4, will be operational shortly. Initial results from the diamond optics are very encouraging. This optical system is the first realization of the Troika principle with subsequent focusing as described by Als-Nielsen (1994). The first structural results from EH3 promise new possibilities of collecting high-resolution diffraction data from extremely large structures. EH4 will be the first station specifically designed for MAD experiments on an undulator beamline at the ESRF. When completed, ID14 will represent 60% of the capacity for macromolecular crystallography at the ESRF.

References

Als-Nielsen, J., Freund, A. K., Grubel, G., Linderholm, J., Nielsen, M., Sanchez del Rio, M. & Sellschop, J. P. F. (1994). *Nucl. Instrum. Methods*, B**94**, 306–318.

Burmeister, W. P., Cottaz, S., Driguez, H., Iori, R., Palmieri, S. & Henrissat, B. (1997). *Structure*, **5,** 663–675.

Cipriani, F., Castagna, J.-C., Claustre, L., Blampey, H., Wilkinson, C., Tomizaki, T., Burmeister, W. P. & Wakatsuki, S. (1997). *ESRF Newsl.* **28**, 30–32.

Collaborative Computational Project, Number 4 (1994). *Acta Cryst.* D**50**, 760–763.

Grübel, G., Als-Nielsen, J. & Freund, A. K. (1994). *J. Phys. IV*, **4**, C9-C27.

Mattenet, M., Schneider, T. & Grübel, G. (1998). *J. Synchrotron Rad.* **5**, 651–653.

Otwinowski, Z. (1993). *Proceedings of the CCP4 Study Weekend*, edited by L. Sawyer, N. Isaacs & S. Bailey, pp. 56–62. Daresbury Laboratory, Warrington, England.

Sanchez del Rio, M. & Dejus, R. J. (1997). *Proc. SPIE*, **3152**, 148–157.

Yamashita, A., Kato, H., Wakatsuki, S., Tomizaki, T., Nakatsu, T., Nakajima, K., Hashimoto, T., Yamada, Y. & Oda, J. (1998). In preparation.